

Four decades of photometry of XX Trianguli, ‘the most spotted star’ in the sky

Zs. Kóvári^{1,2}, K. G. Strassmeier^{3,4}, K. Oláh^{1,2}, B. Seli^{1,2}, G.W. Henry⁵, and K. Vida^{1,2}

¹ Konkoly Observatory, HUN-REN Research Centre for Astronomy and Earth Sciences, Konkoly Thege út 15-17., H-1121 Budapest, Hungary

e-mail: kovari@konkoly.hu

² HUN-REN RCAES, MTA Centre of Excellence, Budapest, Konkoly Thege út 15-17., H-1121 Budapest, Hungary

³ Leibniz-Institute for Astrophysics Potsdam (AIP), An der Sternwarte 16, D-14482 Potsdam, Germany

⁴ Institute for Physics and Astronomy, University of Potsdam, Karl-Liebknecht-Strasse 24/25, D-14476 Potsdam, Germany

⁵ Tennessee State University, Nashville, TN 37209, USA (retired)

Received ...; accepted ...

ABSTRACT

Context. Over the past 40 years the brightness variations of XX Tri, a single line RS CVn type binary system with a synchronized K-giant primary, has exceeded one magnitude in the *V* band. Although these changes are primarily caused by starspots, an additional activity-related mechanism may also be behind the long-term trend of overall brightness increase.

Aims. By compiling the most complete photometric data set so far, we attempt to examine how the nature of seasonal-to-decadal changes can be linked to global magnetism.

Methods. To find the long-term activity cycles and their properties a time-frequency analyser code is used. We divided the entire data set into four consecutive intervals, for which we separately determined the Fourier spectra around the orbital period. This is performed with a Fourier-transformation based frequency analyser tool.

Results. The long-term brightening of XX Tri was accompanied by a gradual increase in the effective temperature, which resulted in a blueing shift in the Hertzsprung-Russell diagram. In the long term, a constant cycle of about 4 years is most strongly present in the entire data. Besides, we also found a modulation of about 11 years, and a slowly decreasing cycle of about 5.7–5.2 years. From the seasonal datasets we found that the most dominant rotation-related periods are scattered around the orbital period. From this we infer a solar-type surface differential rotation, although the surface shear is significantly smaller than that of the Sun.

Conclusions. The 4-year cycle indicates flip-flop-like behavior: during this time, the 2–3 active longitudes usually present on the stellar surface are rearranged. The magnitude-range changes in the long term cannot be interpreted solely as changes in the number and size of spots; the unspotted brightness of XX Tri has also increased over the decades. This should alert users of photometric spot models to reconsider the basic concept of constant unspotted brightness in similar cases.

Key words. stars: activity – stars: late-type – stars: imaging – stars: starspots – Stars: individual: XX Tri

1. Introduction

Dark starspots, first mentioned by Kron (1947), are a long-known feature of cool stars with convective envelopes. A characteristic subgroup of these stars is RS Canum Veneticorum (RS CVn) variables, which are close binaries with a cool component showing chromospheric activity (e.g., starspots). Behind the magnetic activity is the dynamo mechanism, which is essentially activated by the convection of conductive plasma and the rotation of the star. Fast rotation is one of the important conditions for amplifying magnetic activity. In the case of RS CVn type stars with an active cool giant component, the binarity plays a prominent role, namely that in such close binary systems, due to the tidal synchronization, the rotation of the star remains fast, even though blowing up to a giant star would just slow down the rotation. However, tidal forces in such systems not only help maintain fast rotation, but tidal interactions are supposed to modify the operation of magnetic dynamo itself (Holzwarth & Schüssler 2003a,b). Such a manifestation is, for example, when active longitudes form at certain phases fixed to the orbit (e.g., Oláh 2006). On the other hand, in RS CVn binaries, the magnetic activity can feed back on the orbital dynamics, causing or-

biting period changes on the timescale of the activity cycle, as described by the Applegate mechanism (Applegate & Patterson 1987; Applegate 1992). Therefore, it is no exaggeration to say that RS CVn type stars are astrophysical laboratory for studying the effect of binarity on activity and vice versa.

Cool starspots typically cause brightness changes of a few tenths of a magnitude due to the rotation of the active component in an RS CVn system. Although the contribution of the bright faculae is only a small fraction of the total rotational brightness change (in shorter wavelength passbands), in some cases a facular network should be taken into account in order to interpret the so-called color anomaly, when the increasing surface temperature in shorter wavelengths (e.g., in *B* passband) tends to "compensate" the color change due to cool spots (Spruit & Weiss 1986; Pettersen et al. 1992).

The dynamo mechanism operating in the background, which produces starspots and other surface structures, causes changes not only on a rotational but also on a decadal time scale, just like the solar dynamo (although at a different level). Oláh et al. (2014) investigated three overactive spotted K giants (IL Hya, XX Tri, and DM UMa), all of which are members of RS CVn binaries, whose brightness changes are also significant on a ro-

tational and longer time scales. Such large changes in brightness on both time scales cannot be explained simply by putting a mixture of dark spots and bright faculae on the surface. In the cited paper, the authors concluded that the anomalous brightness change on the decadal scale can be explained by a few percent change in the size of the star due to the strong and changing global magnetic field during the activity cycle. However, except in the case of IL Hya, this possible explanation has not yet been confirmed.

In the most extreme case of XX Tri, the rotation-related photometric amplitude reached 0.6 mag in Johnson *V* (Nolthenius 1991), which not only required extremely large and cool spots, but also the distribution of the spots on the stellar surface had to be uneven as well along the rotational phase (for different approaches to light curve modeling see Strassmeier & Oláh 1992; Hampton et al. 1996). In addition, over the past 40 years the long-term peak-to-peak brightness variation of XX Tri has exceeded one magnitude in *V* (cf. Fig. 1 later in this paper). According to this, XX Tri deserves the title of "the most spotted star" in the sky. Our present study is dedicated to study the long-term photometric behaviour of this particularly interesting target.

XX Tri (=HD 12545), a long-period RS CVn system of a bright ($V_{br}=7.64$ mag) K0III active primary component. Its orbital period of ≈ 23.97 days (Bopp et al. 1993; Künstler et al. 2015) is very close to the photometric period around 23.9 ± 0.2 days attributed to starspots on the rotating stellar surface, that is, the system is synchronized. The star, which is otherwise a single-lined spectroscopic binary with an unseen (most probably M-type main sequence) secondary component, has long been known for its strong Ca II H&K emission (Bidelman 1985; Montes et al. 1995). Spectroscopic monitoring of XX Tri showed its H α line consistently in emission (Strassmeier et al. 1990; Bopp et al. 1993; Montes et al. 1997), suggesting an extremely high level of chromospheric activity. Accordingly, XX Tri is also a bright target in ultraviolet (Bopp et al. 1993; Cardini et al. 2003) and possesses a luminous X-ray corona (Dempsey et al. 1997). The lithium abundance was found to be moderately strong, $A(\text{Li}) \approx 1.7$, supporting that XX Tri is a He-core burning red giant branch (RGB) star at the evolutionary stage which can be linked to lithium enrichment (see, e.g., Charbonnel & Balachandran 2000; Kumar et al. 2011; Li et al. 2024, etc.). Moreover, according to Casey et al. (2019) lithium enrichment can even be related to binarity (but on the other hand, see also Jorissen et al. 2020).

Based on precise $UBV(RI)_C$ photometric measurements from 1991 Strassmeier & Oláh (1992) modeled a huge ($\Delta V \approx 0.5$ mag) rotational variability caused by cool starspots. Unspotted brightness was chosen as the brightest value measured up to that time, that is, $V=8.11$ mag (Nolthenius 1991). From the 0.12-mag large amplitude $V-I$ color index, Strassmeier & Oláh (1992) derived a spot temperature of -1100 K relative to the assumed unspotted surface of 4820 K. Also, the spectral type was specified to K0III, instead of G5IV as listed earlier in Strassmeier et al. (1988). The derived spot coverage, however, was so large that the spot model essentially reached the limit where the visible stellar surface barely had any room left to account for the large rotation amplitude *and* the overall long-term brightness change together. If the unspotted *V* brightness was chosen only a few tenths of a magnitude brighter, it would not have been possible to obtain any suitable spot model for the observed light curve. We note here, that knowing the subsequent brightening of the star (see later in this paper), the assumption that there would be an "unchanged" unspotted brightness value over time is obviously not tenable.

The first Doppler image of the star was presented by Strassmeier (1999) in the turn of 1997/98, the season characterized by high-amplitude changes in brightness. For the extreme rotational variability, the Doppler reconstruction required a gigantic high-latitude cool spot, but also bright areas in the opposite hemisphere. The star's then-record brightness and record photometric amplitude were reminiscent of the solar activity, in that our Sun is also the brightest when the degree of spot coverage is the greatest (i.e., at the maximum of the solar cycle).

In our subsequent, more extensive Doppler study (Künstler et al. 2015), we managed to obtain 36 Doppler images based on continuous spectroscopic observations spanning six years, collected with the help of the STELLA robotic observatory at Tenerife, Spain. According to the study, the surface of XX Tri was covered by large, high-latitude and even polar spots and occasionally smaller equatorial spots. Furthermore, based on the time-series Doppler images it was possible to monitor the morphological changes of the spots. The measured spot decay rate provided a basis for estimating the turbulent diffusivity. However, since it was not possible to separate the opposite processes occurring together (i.e., spot decay and formation), the derived value of the turbulent diffusivity may need a revision.

In our most recent work (Strassmeier et al. 2024, hereafter Paper I) we presented a time series Doppler imaging study of XX Tri, covering 16 years (2006-2022, including the six years of data from the previous study). From this most comprehensive Doppler imaging study so far, in which 99(!) Doppler images were reconstructed from the same target, it was concluded that *i*) the stellar dynamo working in the background is aperiodic, likely chaotic in nature; *ii*) the Doppler images indicate "missing" (i.e. blocked) flux due to cool spots of up to 10% of the total flux, which is redistributed on a global scale, contributing to an increase in the effective temperature on a longer timescale; *iii*) the rotation-induced stellar photocenter variations due to starspots pose an intrinsic limitation for astrometric exoplanet catches. However, the Doppler study only covers less than half of the available photometric time series, overlapping essentially with the most recent period during which XX Tri is at its brightest state. In comparison, at the very beginning of the systematic photometric observations, the star was fainter by about 0.65 mag on average in *V*, while its rotation amplitude was three-four times that of today. This significant difference can definitely be linked to the change in processes related to global magnetism over decades, that is, to the change in dynamo operation. Therefore, in the present paper, we focus on the analysis of the most complete long-term photoelectric photometric datasets available from the past approximately four decades, obtained mostly with automatic photoelectric telescopes (hereafter APTs). Below we adopt from Paper I the most thorough summary of the stellar parameters so far, which we list in Table 1.

This paper is organized as follows: we present our available photometric data in Sect. 2 and the methods used in Sect. 3. The seasonal photometric period changes are analyzed in Sect. 4.1, long-term cycles are investigated in Sect. 4.2, while the long-term color changes are presented and interpreted in Sect. 4.3. Our basic results are discussed in Sect. 5 and summarized in Sect. 6.

2. Observations

For our study, we attempted to collect all available photometric data about XX Tri. All published photometric data from the literature were gathered and used. Sources of the observations until 1996 are listed in Strassmeier et al. (1997, see their Table 5),

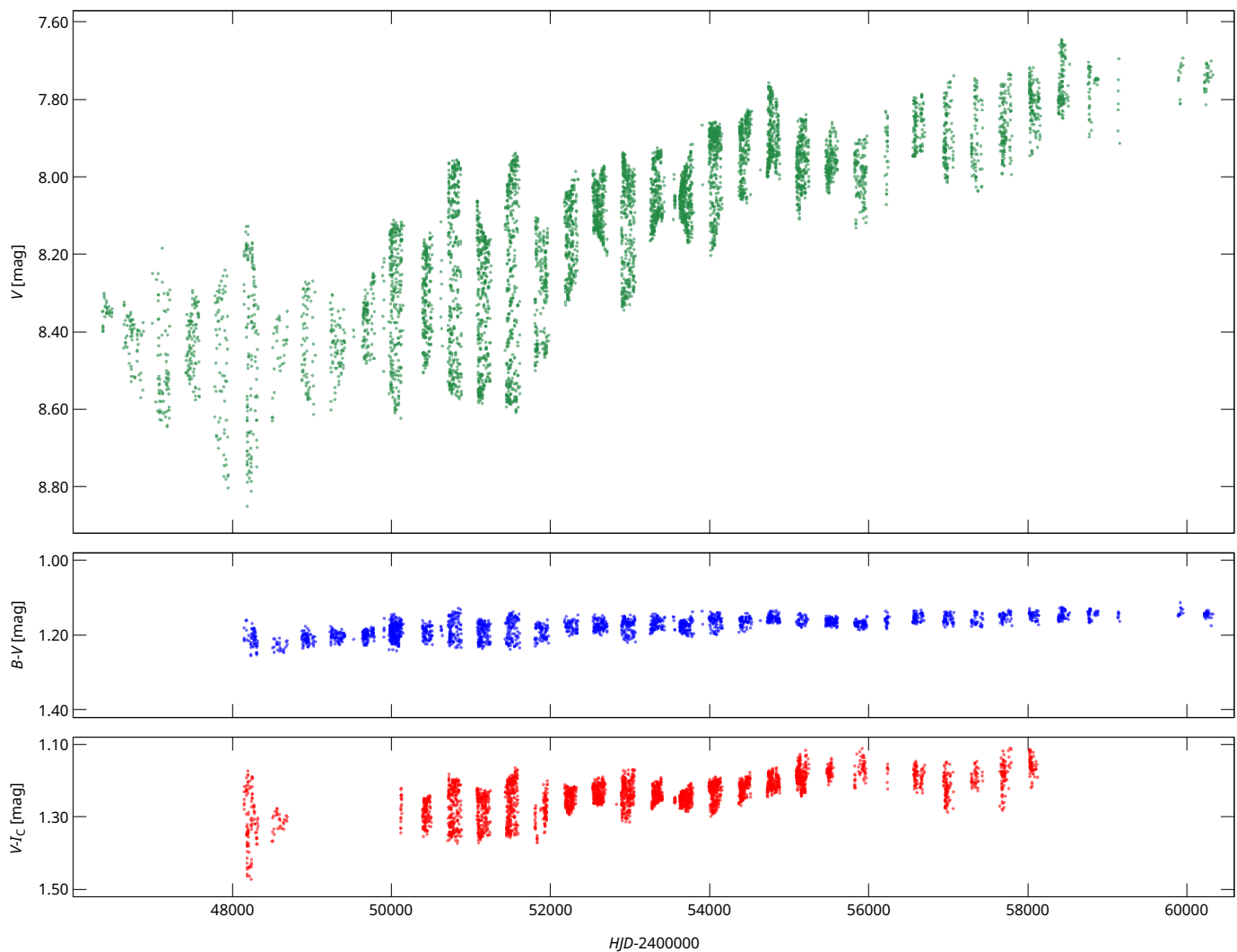


Fig. 1. Combined V , $B - V$ and $V - I_C$ data of XX Tri that we use in this paper.

and the corresponding data can be found in the VizieR online catalog of the Strasbourg astronomical Data Center (CDS). Unpublished data referred as "private communication" in the above paper, including the $UBV(RI)_C$ data from Konkoly Observatory, have been uploaded to the VizieR catalog as a supplement to this paper.

Most of the B , V observations were made by the Tennessee State University T3 0.41-m Automated Photometric Telescope (APT) located at Fairborn Observatory, Arizona, USA (Henry 1995); this series of observations ended in 2024. The V observations made between 1990 October and 2015 February have been published in Jetsu et al. (2017). Now all XX Tri data from T3 have been compiled and uploaded to the VizieR online catalog.

Fairborn Observatory gave place to two more APTs used for XX Tri photometry, the Wolfgang (T6) and Amadeus (T7) 0.75-m automatic twin telescopes, which were jointly operated initially by the University of Vienna and later by Leibniz-Astrophysical Institute Potsdam (AIP). The Wolfgang photometer is optimized for Strömgren $uvby$. The Amadeus photometer is optimized for the Johnson BVR system. The Wolfgang system was available for XX Tri from 1997 to 2009. Unfortunately, however, the photometric performance of Amadeus was not satisfactory in the following ten years either. After the cathode tube was replaced with a blue-sensitive one in 13 January 2018

($JD\ 2458132$), the system performed better for a short time, but faded again shortly afterwards. The telescope finally ended its operation in January 2019. We note that the photometric data collected with the T6-T7 telescopes have already been published in a supplement to Paper I¹

The combined most complete V , $B - V$ and $V - I_C$ data of XX Tri are shown in Fig. 1. To convert differential measurements to absolute scale, HD 12478 was used as a comparison star with magnitudes $V=7^m78$, $B - V=1^m45$, and $V - I_C=1^m38$.

3. Methods

3.1. Period search by MuFrAn

The period search analysis of the light curves is partially performed with the MuFrAn (Multi-Frequency Analyzer, Csubry & Kolláth 2004) code. This Fourier-transformation based frequency analyser tool is suitable for searching for multiple periods in unevenly sampled time series and displaying the results graphically. We use MuFrAn to investigate fluctuations in the rotation period over several seasons (Sect. 4.1).

¹ Available at https://data.aip.de/projects/xx_tri.html

Table 1. Relevant astrophysical data of XX Tri adopted from Paper I.

Parameter	Value
Spectral type	K0III
Distance [pc]	196.3 ± 1.1
V_{br} [mag]	7.64
Average ($V - I_C$) [mag]	1.18
P_{rot} [d] ^a	23.470 – 24.716
P_{orb} [d]	23.9674 ± 0.0005
Inclination [°]	60 ± 10
$v \sin i$ [kms ⁻¹]	20.0 ± 0.6
T_{eff} [K] ^b	4627 ± 26
log g (cgs)	2.82 ± 0.05
Metallicity [Fe/H]	-0.13 ± 0.04
Radius [R_{\odot}] ^c	$10.95^{+1.4}_{-0.95}$
Radius [R_{\odot}] ^d	8.95 ± 0.23
Luminosity [L_{\odot}] ^d	337 ± 2
Mass [M_{\odot}]	$1.1^{+0.2}_{-0.3}$
Age [Gyr]	$7.4^{+2.3}_{-3.2}$

Notes.

- (^a) This paper, extreme values, cf. Fig. 2 and Table 2;
(^b) From fitting 16 years of spectroscopic data with synthetic spectra;
(^c) Derived from $v \sin i$, P_{rot} , and i ;
(^d) Derived from V_{br} , T_{eff} , and Gaia DR3 parallax.

Looking for the possible variability of the rotational modulation, first, the high amplitude, long-term changes were simultaneously refined with Discrete Fourier Transform (DFT, Deeming 1975) and removed from the data. The dataset prewhitened in this way was analysed again in its full length and then divided into separate subsets. We note that prewhitening is not of great importance in our case, as it has no effect in the frequency range typical of the rotation.

3.2. Time-frequency analysis by TiFrAn

To find the activity cycles and their properties the program package TiFrAn (Time-Frequency Analysis, Kolláth & Oláh 2009) has been used. Since the amplitude of the rotational modulation shown by the observations were grossly variable, exceeding 0.6 magnitudes sometimes, we removed the rotational signals from the unevenly sampled seasonal light curves. This way we could avoid false signals in the analysis targeting decadal variability. The program package can operate with different kernels like the short-term Fourier Transform (STFT) and the Choi-Williams kernel (CWD), which has a better frequency resolution but less time resolution. A detailed description of the practical application of this tool to long-term time series of stars can be found in Oláh et al. (2009, see their Sect. 3).

4. Results

4.1. Seasonal changes in the rotation period

In the case of spotted stars, a known phenomenon is the temporal change of the rotation signal, which is mostly explained by the changing spot configuration from season to season, as well as differential rotation. On the one hand, it would be desirable to examine as short time intervals as possible (e.g., annual), but on the other hand, deriving a precise period is only possible in the case of a sufficiently long data series. Since during an annual observing season our data cover roughly 10-12 rotation

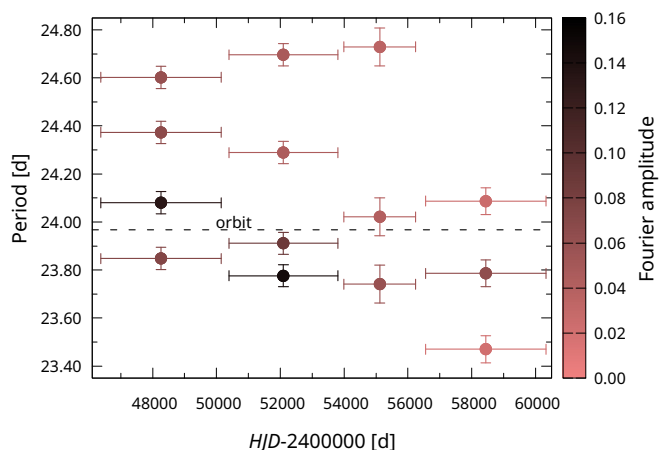


Fig. 2. Rotational periods of XX Tri for four segments of the V dataset. The orbital period is indicated with a dashed line. The dots marking the detected rotational signals of each segment are colored according to their Fourier amplitudes. See also Table 2.

periods at most, period search for each year is not possible. Instead, we divided the data into four segments of similar length, keeping in mind that no significant changes occur within each segment, in the sense that the trend or "dynamics" of change are roughly "constant" within a segment. With the division according to this principle, the following time intervals were created ($HJD - 2400000$): 46370-50152 (nearly constant average brightness), 50391-53804 (continuous increase in average brightness), 53995-56244 (average brightness reaches its local maximum and then decreases), and 56555-60327 (slight upward trend in average brightness); cf. the upper panel of Fig. 1.

The period search was carried out as follows. Using MufrAn, we searched for the most dominant rotation-related period from data previously cleaned of long-term trends. The next period search was always performed on the spectrum prewhitened by the previously found dominant period, and so on until no period of reasonable amplitude remains. The resulting 3-4 periods per season with their respective Fourier amplitudes are listed in Table 2 for all four intervals, which are graphically represented in Fig. 2 in comparison with the orbital period.

We note that in the classical approach, according to the uncertainty principle, $\Delta w \Delta t \geq 1$ relation applies between the Δw width of the Fourier signal and the Δt length of the dataset. Based on this, the uncertainty of the Fourier signals obtained for the different seasons (frequency converted to days) would be on the order of ~ 0.15 - 0.20 d. However, this value overestimates the more realistic uncertainties that can be derived from the peak widths measured at 90% heights of the peaks in the amplitude spectra (cf. Oláh et al. 2003). In comparison with the obtained periods and their associated errors, we also present the Lomb-Scargle periodograms obtained for the entire V data and the four sub-seasons in Appendix A. The most dominant periods in Fig. 2 scatter around the orbital period, while those with smaller amplitudes usually diverge more. Possible reasons for this are discussed in Sect. 5.

4.2. Long-term brightness changes

Long-term, cycle-like brightness variation with a characteristic time-scale of about 4 years of XX Tri has been derived for a 21 years long dataset by Oláh et al. (2009) using TiFrAn. The present photometric dataset spans now four decades for which

Table 2. Seasonal rotational periods and their corresponding Fourier amplitudes.

46370-50152 ^a		50391-53804 ^a		53995-56244 ^a		56555-60327 ^a	
period [d] ^b	amplitude	period [d] ^b	amplitude	period [d] ^c	amplitude	period [d] ^d	amplitude
24.080	0.13268	23.776	0.14665	23.741	0.05881	23.786	0.06398
23.848	0.07256	23.911	0.08768	24.021	0.04071	24.087	0.02494
24.373	0.06623	24.696	0.04672	24.729	0.03543	23.470	0.02083
24.602	0.06005	24.289	0.04480	–	–	–	–

Notes. ^(a) $HJD-2400000$; ^(b) Accuracy limit ± 0.046 d; ^(c) Accuracy limit ± 0.079 d; ^(d) Accuracy limit ± 0.056 d.

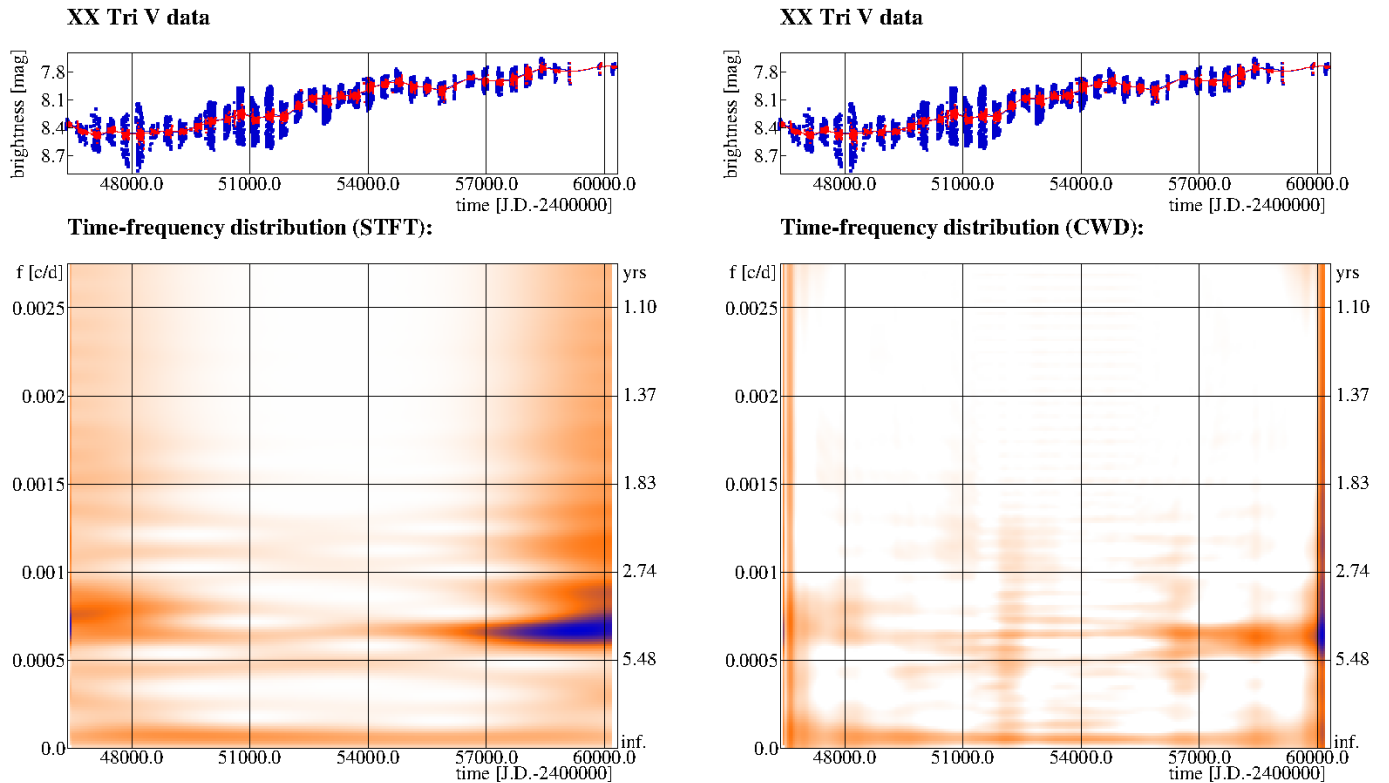


Fig. 3. Time-frequency plot of the long-term variability of XX Tri over four decades using STFT (lower left panel) and CWD (lower right panel) kernels. In the two upper (in this case identical) panels, the blue dots show the original V magnitudes, and the blue line shows their spline fit, while the red dots represent the data cleaned of the rotational signal, and the red line represents the corresponding spline fit.

we repeated the time-frequency analysis. First, the rotational modulation was removed from the data since the uneven distribution of the measured datapoints and the sometimes very high amplitude could alter the seasonal variations giving rise of possible false long-term signals. The result of the long-term variability with STFT is plotted in the left panel of Fig. 3, while using CWD with better frequency but poorer time resolution, is seen in the right panel of Fig. 3.

Apart from the visible, very high amplitude brightening during the time-span of ~ 40 years, a modulation in the order of ≈ 11 years, a slowly decreasing cycle between ≈ 5.7 - 5.2 years and a constant cycle of about 4 years are present in the data throughout the observations, the latter being the strongest signal of all.

4.3. Migration on the HRD

Long-term BVI_C dataset is used to trace the temperature changes on the surface of XX Tri. The bulk of the dataset consists of independent series in B , V and V, I_C colors by different automated telescopes (see Sect. 2), supplemented with a small amount of

data gathered from other sources. As Fig. 5 shows, the agreement between the two sets of V measurements made by different telescopes is excellent, apart from an about $0^m.05$ discrepancy between HJD 2455478 and 2455970, for unknown reason to us. This, however, translates to about 80 K temperature difference which is not negligible. The right panel of Fig. 5 shows the shifted V data and the corresponding shifted $V - I_C$ values (all of the original color index data are shown in Fig. 1).

The color index data ($B - V, V - I_C$) were corrected for interstellar extinction to define temperatures. For getting the extinction parameter we accessed the 3D dust maps of interstellar dust reddening² (Bayestar17, Green et al. 2018). According to the best-fit distance-reddening curve we adopt a color excess of $E(B - V) = 0.05^{+0.02}_{-0.03}$ (cf. Oláh et al. 2014, see also their Fig. 4), along with $E(V - I_C)/E(B - V) = 1.25$ from Fitzpatrick (1999).

Surface temperatures were estimated using the empirical color-temperature calibration of Worthey & Lee (2011) by interpolating their table to the the measured color index values

² <http://argonaut.skymaps.info/>

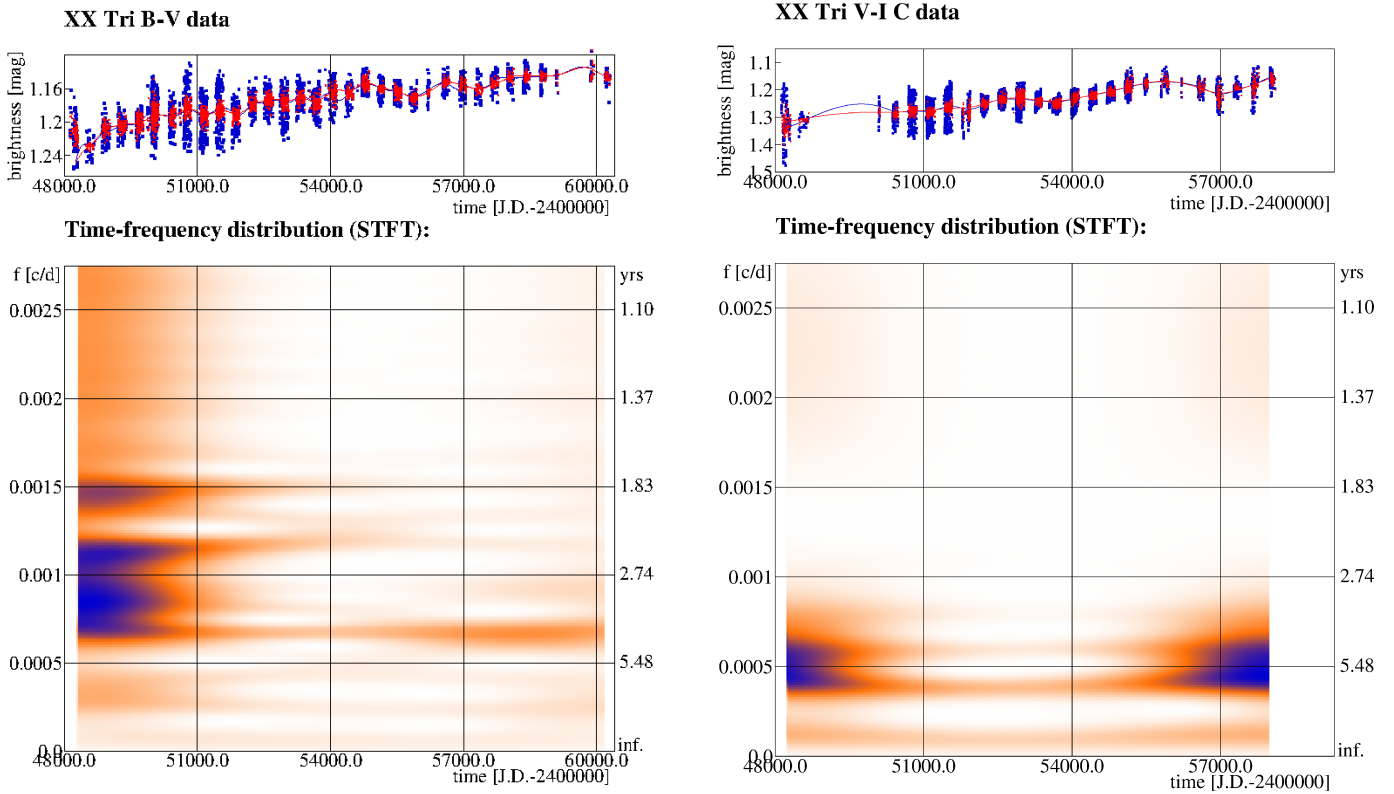


Fig. 4. Time-frequency plot of the long-term variability of XX Tri over nearly four decades in $B - V$ (left panels) and $V - I_C$ color indices (right panels). Otherwise as in Fig. 3.

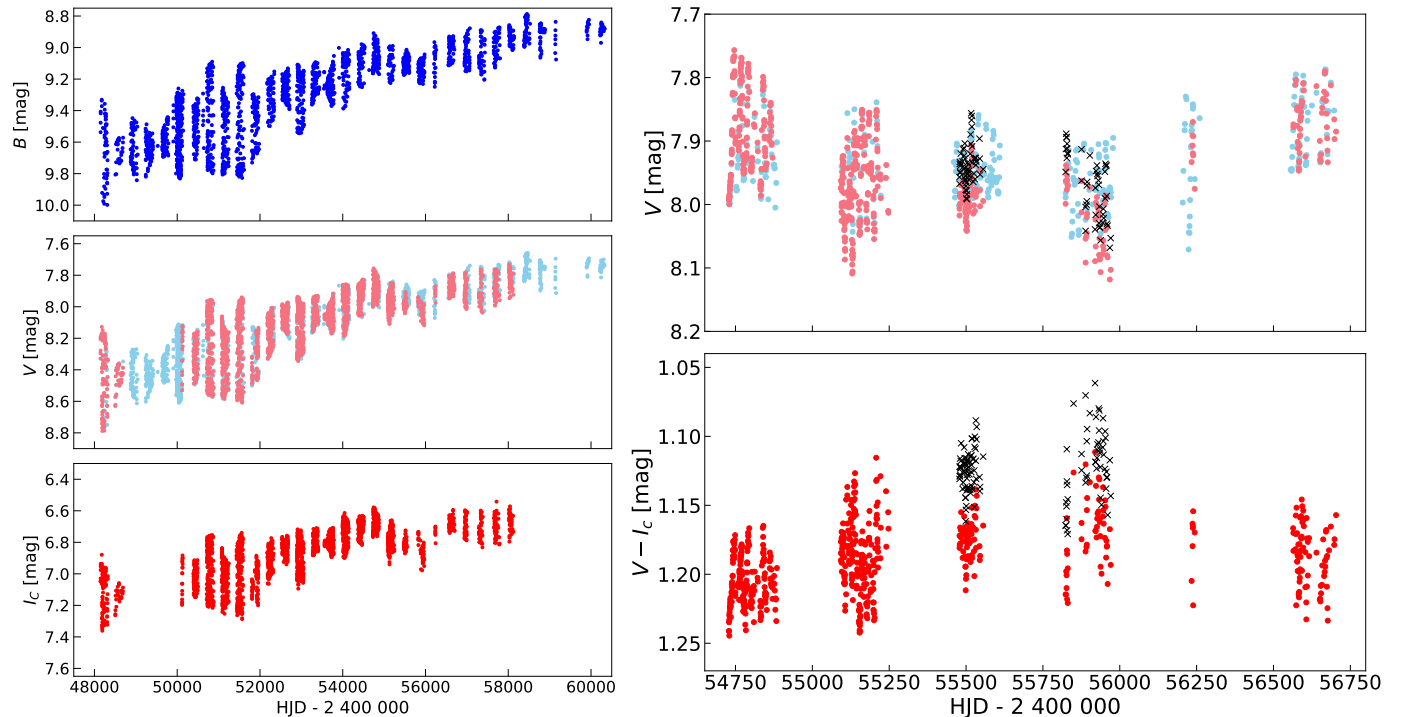


Fig. 5. Left, from top to bottom: B , V and I_C data used for temperature determinations. In the middle panel showing V data, points measured simultaneously with B measurements are marked in light blue, and points measured simultaneously with I_C measurements are marked in light red. Right: enlarged view around the discrepant V (upper panel) and $V - I_C$ (lower panel) data; data points corrected by $0^{\text{m}}05$ are indicated by black crosses (for details see the first paragraph of Sect. 4.3).

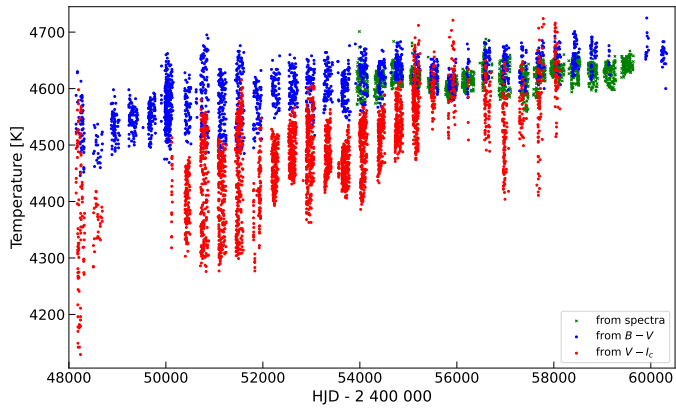


Fig. 6. Comparison of the overall stellar temperature variations derived from the STELLA spectra used in Paper I (green crosses) and from $B-V$ (blue dots) and $V-I_C$ color indices (red dots).

corrected for the interstellar extinction and the surface gravity ($\log g = 2.82$) and metallicity ($[\text{Fe}/\text{H}] = -0.13$). For the second half of the available color-temperature data we have surface temperature values obtained from spectral synthesis of 1822 spectra (Paper I). The results are plotted in Fig. 6.

The substantial variability of the surface temperature in the order of about 500 K seen in Fig. 6, apart from the interstellar extinction, affect the position of XX Tri in the HRD as was already shown in Oláh et al. (2014). Here we present stellar surface temperatures derived from $B-V$ and $V-I_C$ color indices. The paths of the star on the HRD in the course of the decades long variation according to the two series of temperature values are plotted in Fig. 8.

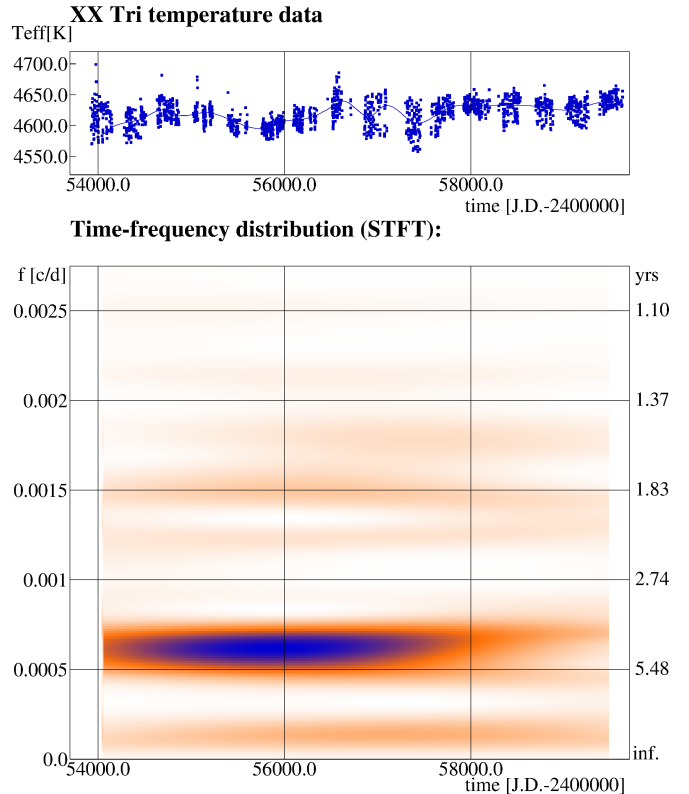


Fig. 7. Variability over 16 years of the spectroscopically determined effective temperature of XX Tri taken from Paper I. Otherwise as in Fig. 3.

5. Discussions

5.1. Long-term periods

It is widely known that in (otherwise usually tidally locked) RS CVn systems, activity cycles are typically anharmonic (e.g. Lanza 2010, see also the references therein), and in many cases, multiple and variable quasi-cycles can be found (Oláh et al. 2009). The photometric data of XX Tri perfectly support this observation: we see a main ~ 4 -year cycle that varies slightly over time, as well as a ~ 6.5 -year cycle that appears spectacularly in the $V-I_C$ color index and although weaker, it is also present in the $B-V$ data (see Fig. 4). In the latter (longer) data series, a ~ 11 -year cycle, the double of 6.5 years, can also be detected. We note that the only cycle-like variation found earlier by Oláh et al. (2009) in their 21 year-long photometric dataset was 3.8 years long, very close to our ~ 4 -year main cycle. We also note that, even though the $B-V$ and $V-I_C$ color index data are 5 and

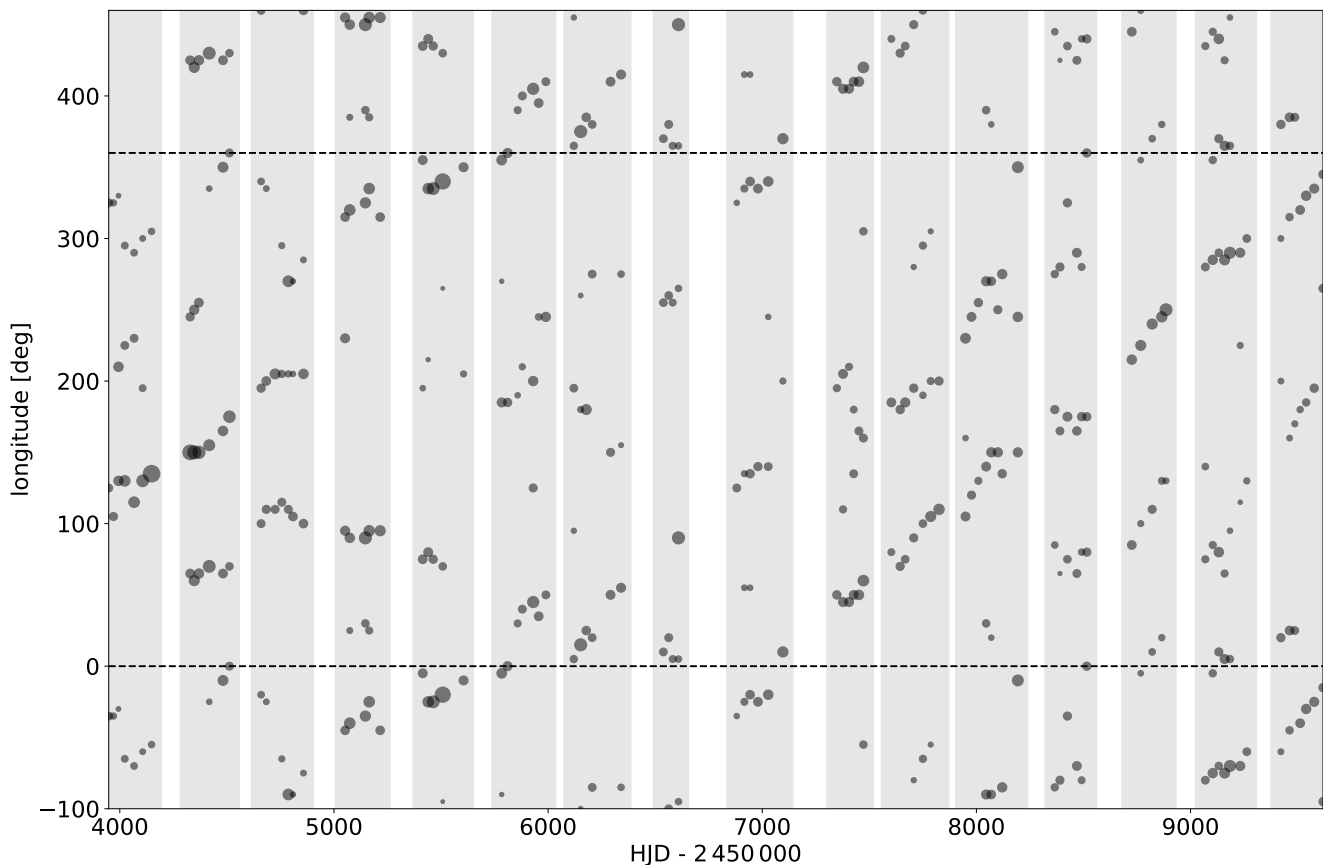


Fig. 9. Longitudes of the activity centers derived from 16 years of time-series Doppler images. We identified two or three activity centers per image. The larger the dot size, the more dominant the active longitude. Vertical gray bars indicate the separate observing seasons.

the photometric observations, more precisely during the high-amplitude period around $\sim HJD$ 2450820 (i.e., 1998), the only reconstructed Doppler image revealed a huge asymmetric polar cap (Strassmeier 1999), while the time-series Doppler imaging study in Paper I, in which the spectroscopic data essentially overlap with the second half of the photometric data, shows that the centroids of the spots are typically located around latitudes between 45° and 65° , but the spots do not extend so far as to cover the visible pole.

To further confirm the operation of solar-type surface differential rotation on XX Tri, using the time-series Doppler images from Paper I, we applied the method of average cross-correlations, a well-established technique dubbed ACCORD (e.g., Kóvári et al. 2012, 2015, 2017b) for detecting surface shear on spotted stars. ACCORD combines information from spot displacements on successive Doppler images to detect and measure surface differential rotation. As shown in Fig. 10, the method results in a grand average correlation pattern clearly indicating a weak sun-like shear. Fitting the pattern by a rotation law in the usual form $\Omega(\beta) = \Omega_{\text{eq}}(1 - \alpha \sin^2 \beta)$, where $\Omega(\beta)$ is the angular velocity measured at latitude β , yields a value of 0.014 ± 0.003 for the shear coefficient α . We draw attention to the fact that the α value obtained from the time-series Doppler images, although smaller, does not contradict the $\Delta P/\bar{P} \approx 0.05$ value given above based purely on photometry, as the latter is only a rough estimate of the relative shear. Finally, we note that in our upcoming paper we are preparing to present a more detailed study focusing on the meanwhile expanded number of time-series Doppler

images and further findings that can be drawn from them (e.g., regarding differential rotation).

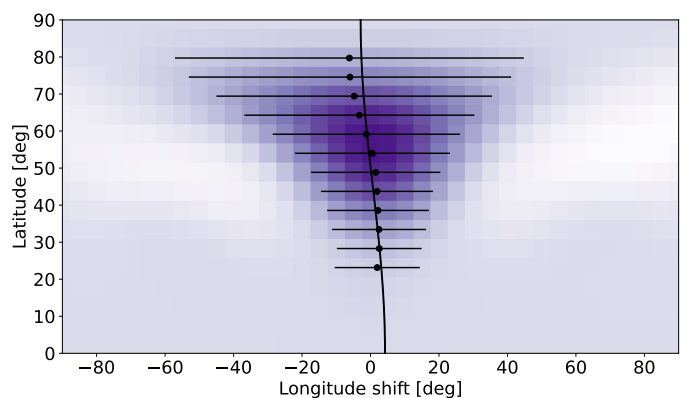


Fig. 10. Grand average of the cross-correlation function maps obtained from ACCORD. The map indicates how much longitude shift occurs at a given latitude due to surface shear over 35 days (the median time interval between successive Doppler maps). The solid line is a sun-like differential rotation fit with a shear coefficient of $\alpha = 0.014$.

5.3. Spot dominated magnetic activity

In the past four decades, XX Tri essentially became hotter and bluer, resulting in a gradual displacement in the red clump region of the HRD; see Fig. 8. This global change is spot-dominated,

meaning that huge, dark starspots dominate the variability. When we see more spots, the star is fainter overall, unlike the plage-dominated Sun, whose activity is characterized by the exact opposite: the Sun is brightest at spot maximum. Another characteristic feature of spot dominance is that there is an anti-correlation between the rotational light curve and the chromospheric activity indicators (e.g. Ca II H&K lines or H α emission). We note that this kind of spot dominance is a regular feature of active (sub)giants in long-period RS CVn systems; we only mention the most well-known such targets here: II Peg and λ And (Frasca et al. 2008; Adebali et al. 2025), IM Peg (Zellem et al. 2010), V711 Tau (Vogt et al. 1999), σ Gem (Kóvári et al. 2001), ζ And (Kóvári et al. 2007; Roettenbacher et al. 2016), etc.

We believe that the significant overall brightness increase of XX Tri observed over the past four decades together with the color index changes, which also cause the displacement of the star on the HRD, are due to strong and variable surface magnetic fields present throughout the intensity variations of surface spot activity (for two more examples see Oláh et al. 2014). All these changes, with the huge amplitudes in the early period and their decreasing magnitude over time, and the gradual brightening, are difficult to interpret other than that the star's unspotted temperature has also increased over the past four decades. The likely cause of this is the extensive spot activity itself, which blocks the outward energy flux, which eventually, on a longer timescale, breaks through and manifests itself in a global brightening (cf. Strassmeier et al. 2024, see their Discussion section).

6. Summary and conclusions

This study is a continuation, the second part of the series of papers that began with the recently published Paper I, which presented an unprecedented Doppler imaging study of XX Tri, visualizing the continuous surface spot evolution for 16 years. In the present 'Paper II' we attempted to perform a comprehensive analysis of the star's four-decade photometric history. Our main conclusions drawn from the results are the following:

1. The most significant of the longer-term cycles appearing in photometric data series is ≈ 4 years, consistent with the 4.1-year cycle found from independent spectroscopic time series in Paper I. This mid-term cycle apparently has nothing to do with the star's gradual brightening over several decades. This cycle indicates rather a flip-flop-like behavior. Compared to the time-series Doppler images of Paper I, it appears that typically during this time the 2-3 active longitudes that are usually present on the stellar surface are rearranged.
2. Comparing the seasonal changes in the rotation period with the results of previous Doppler studies suggests that XX Tri performs solar-like surface differential rotation, although the surface shear is significantly smaller than that of the Sun. This is further supported by the weak, sun-like differential rotation with a shear coefficient of $\alpha = 0.014$, inferred from a preliminary analysis of the time-series Doppler images from Paper I. Our result is in good agreement with the empirically predicted value for such giant components in RS CVn type close binary systems.
3. The average brightness of the star has gradually increased over the four decades of observation, while the spot coverage and the seasonal amplitudes of the brightness variability in general have decreased. However, the observed changes cannot be interpreted solely as changes in the number and size of the spots, we must also assume that the surface temperature, that is the unspotted brightness, has also increased over

the decades. This result should prompt users of photometric spot models to reconsider the basic concept of a constant unspotted temperature when interpreting long-term trends in brightness changes of spotted stars.

Data availability

The previously unpublished photometric data of XX Tri used in this paper (listed in Sect. 2) are available in electronic form at the CDS via anonymous ftp to cdsarc.u-strasbg.fr (130.79.128.5) or via <http://cdsweb.u-strasbg.fr/cgi-bin/qcat?J/A+A/>.

Acknowledgements. The authors gratefully acknowledge the comments and suggestions of the reviewer, Dr S. Gu, which helped improve the paper. This work was supported by the Hungarian National Research, Development and Innovation Office grant KKP-143986. GWH acknowledges long-term support from NASA, NSF, and the Tennessee State University. STELLA was made possible by funding through the State of Brandenburg (MWFK) and the German Federal Ministry of Education and Research (BMBF). The facility is a collaboration of the AIP in Brandenburg with the IAC in Tenerife. This work has made use of data from the European Space Agency (ESA) mission *Gaia* (<https://www.cosmos.esa.int/gaia>), processed by the *Gaia* Data Processing and Analysis Consortium (DPAC, <https://www.cosmos.esa.int/web/gaia/dpac/consortium>). Funding for the DPAC has been provided by national institutions, in particular the institutions participating in the *Gaia* Multilateral Agreement.

References

- Adebali, Ö., Strassmeier, K. G., Ilyin, I. V., et al. 2025, A&A, 695, A89
 Applegate, J. H. 1992, ApJ, 385, 621
 Applegate, J. H. & Patterson, J. 1987, ApJ, 322, L99
 Arlt, R. & Weiss, N. 2014, Space Sci. Rev., 186, 525
 Bidelman, W. P. 1985, International Amateur-Professional Photoelectric Photometry Communications, 21, 53
 Bopp, B. W., Fekel, F. C., Aufdenberg, J. P., Dempsey, R., & Dadonas, V. 1993, AJ, 106, 2502
 Cardini, D., Cassatella, A., Badiali, M., Altamore, A., & Fernández-Figueroa, M. J. 2003, A&A, 408, 337
 Casey, A. R., Ho, A. Y. Q., Ness, M., et al. 2019, ApJ, 880, 125
 Charbonnel, C. & Balachandran, S. C. 2000, A&A, 359, 563
 Csabry, Z. & Kolláth, Z. 2004, in ESA Special Publication, Vol. 559, SOHO 14 Helio- and Asteroseismology: Towards a Golden Future, ed. D. Danesy, 396
 Deeming, T. J. 1975, Ap&SS, 36, 137
 Dempsey, R. C., Linsky, J. L., Fleming, T. A., & Schmitt, J. H. M. M. 1997, ApJ, 478, 358
 Fitzpatrick, E. L. 1999, PASP, 111, 63
 Frasca, A., Biazzo, K., Taş, G., Evren, S., & Lanzafame, A. C. 2008, A&A, 479, 557
 Green, G. M., Schlafly, E. F., Finkbeiner, D., et al. 2018, MNRAS, 478, 651
 Hampton, M., Henry, G. W., Eaton, J. A., Nolthenius, R. A., & Hall, D. S. 1996, PASP, 108, 68
 Henry, G. W. 1995, in Astronomical Society of the Pacific Conference Series, Vol. 79, Robotic Telescopes. Current Capabilities, Present Developments, and Future Prospects for Automated Astronomy, ed. G. W. Henry & J. A. Eaton, 37
 Holzwarth, V. & Schüssler, M. 2003a, A&A, 405, 291
 Holzwarth, V. & Schüssler, M. 2003b, A&A, 405, 303
 Jetsu, L., Henry, G. W., & Lehtinen, J. 2017, ApJ, 838, 122
 Jorissen, A., Van Winckel, H., Siess, L., et al. 2020, A&A, 639, A7
 Kóvári, Zs., Bartus, J., Strassmeier, K. G., et al. 2007, A&A, 463, 1071
 Kóvári, Zs., Korhonen, H., Kriskovics, L., et al. 2012, A&A, 539, A50
 Kóvári, Zs., Kriskovics, L., Künstler, A., et al. 2015, A&A, 573, A98
 Kóvári, Zs., Oláh, K., Kriskovics, L., et al. 2017a, Astronomische Nachrichten, 338, 903
 Kóvári, Zs., Strassmeier, K. G., Bartus, J., et al. 2001, A&A, 373, 199
 Kóvári, Zs., Strassmeier, K. G., Carroll, T. A., et al. 2017b, A&A, 606, A42
 Kóvári, Zs., Strassmeier, K. G., Kriskovics, L., et al. 2024, A&A, 684, A94
 Kolláth, Z. & Oláh, K. 2009, A&A, 501, 695
 Kron, G. E. 1947, PASP, 59, 261
 Kumar, Y. B., Reddy, B. E., & Lambert, D. L. 2011, ApJ, 730, L12
 Künstler, A., Carroll, T. A., & Strassmeier, K. G. 2015, A&A, 578, A101

- Lanza, A. F. 2010, in IAU Symposium, Vol. 264, Solar and Stellar Variability: Impact on Earth and Planets, ed. A. G. Kosovichev, A. H. Andrei, & J.-P. Rozelot, 120–129
- Li, X.-F., Shi, J.-R., Li, Y., Yan, H.-L., & Zhang, J.-H. 2024, MNRAS, 529, 1423
- Marsden, S. C., Berdyugina, S. V., Donati, J. F., Eaton, J. A., & Williamson, M. H. 2007, *Astronomische Nachrichten*, 328, 1047
- Montes, D., de Castro, E., Fernandez-Figueroa, M. J., & Cornide, M. 1995, *A&AS*, 114, 287
- Montes, D., Fernandez-Figueroa, M. J., de Castro, E., & Sanz-Forcada, J. 1997, *A&AS*, 125, 263
- Nolthenius, R. 1991, *Information Bulletin on Variable Stars*, 3589, 1
- Oláh, K. 2006, *Ap&SS*, 304, 145
- Oláh, K., Jurcsik, J., & Strassmeier, K. G. 2003, *A&A*, 410, 685
- Oláh, K., Kolláth, Z., Granzer, T., et al. 2009, *A&A*, 501, 703
- Oláh, K., Moór, A., Kővári, Zs., et al. 2014, *A&A*, 572, A94
- Özdarcan, O., Carroll, T. A., Künstler, A., et al. 2016, *A&A*, 593, A123
- Petit, P., Donati, J. F., Wade, G. A., et al. 2004, MNRAS, 348, 1175
- Pettersen, B. R., Hawley, S. L., & Fisher, G. H. 1992, *Sol. Phys.*, 142, 197
- Roettenbacher, R. M., Monnier, J. D., Korhonen, H., et al. 2016, *Nature*, 533, 217
- Spiegel, E. A. 2009, *Space Sci. Rev.*, 144, 25
- Spruit, H. C. & Weiss, A. 1986, *A&A*, 166, 167
- Strassmeier, K. G. 1999, *A&A*, 347, 225
- Strassmeier, K. G., Bartus, J., Cutispoto, G., & Rodono, M. 1997, *A&AS*, 125, 11
- Strassmeier, K. G., Fekel, F. C., Bopp, B. W., Dempsey, R. C., & Henry, G. W. 1990, *ApJS*, 72, 191
- Strassmeier, K. G., Hall, D. S., Zeilik, M., et al. 1988, *A&AS*, 72, 291
- Strassmeier, K. G., Kővári, Zs., Weber, M., & Granzer, T. 2024, *Nature Communications*, 15, 9986 (Paper I)
- Strassmeier, K. G. & Oláh, K. 1992, *A&A*, 259, 595
- Vogt, S. S., Hatzes, A. P., Misch, A. A., & Kürster, M. 1999, *ApJS*, 121, 547
- Weber, M. 2007, *Astronomische Nachrichten*, 328, 1075
- Worthey, G. & Lee, H.-c. 2011, *ApJS*, 193, 1
- Xiang, Y., Gu, S., Collier Cameron, A., Barnes, J. R., & Cao, D. 2024, *ApJ*, 976, 217
- Zellem, R., Guinan, E. F., Messina, S., et al. 2010, *PASP*, 122, 670

Appendix A: Lomb-Scargle periodograms

In connection with Fig. 2 and Table 2, we present here the Lomb-Scargle periodograms obtained for the entire V data set (see Fig. A.1) and the four sub-seasons (see Fig. A.2). We note that the amplitudes of the periodograms presented here do not necessarily match the final values in Table 2, as those in the table were derived from the successive uses of the `MuFrAn` code (see Sect. 3), in which the next period search was always performed on the spectrum prewhitened by the previously found dominant period. Nevertheless, the locations of the relevant Lomb-Scargle peaks agree well with the corresponding period values in Table 2.

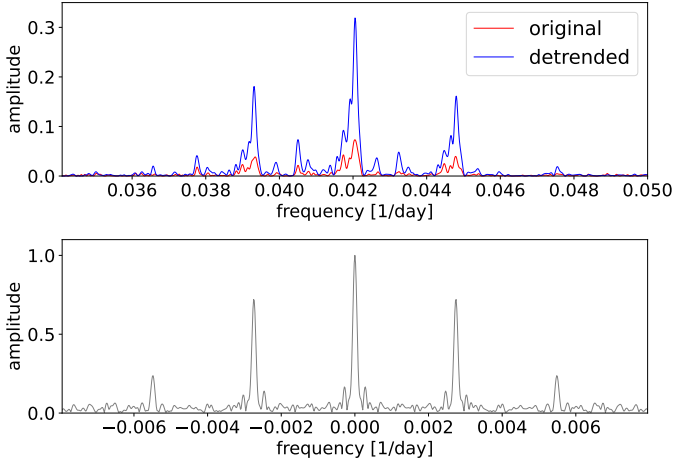


Fig. A.1. Top panel: part of the Lomb-Scargle periodogram for the entire V data showing the rotation-related periods. The highest peak of the main lobe corresponds to the strongest period of ≈ 23.78 d, the other two large lateral ones (and the other much smaller ones) are side lobes from windowing. Bottom panel: the corresponding window function.

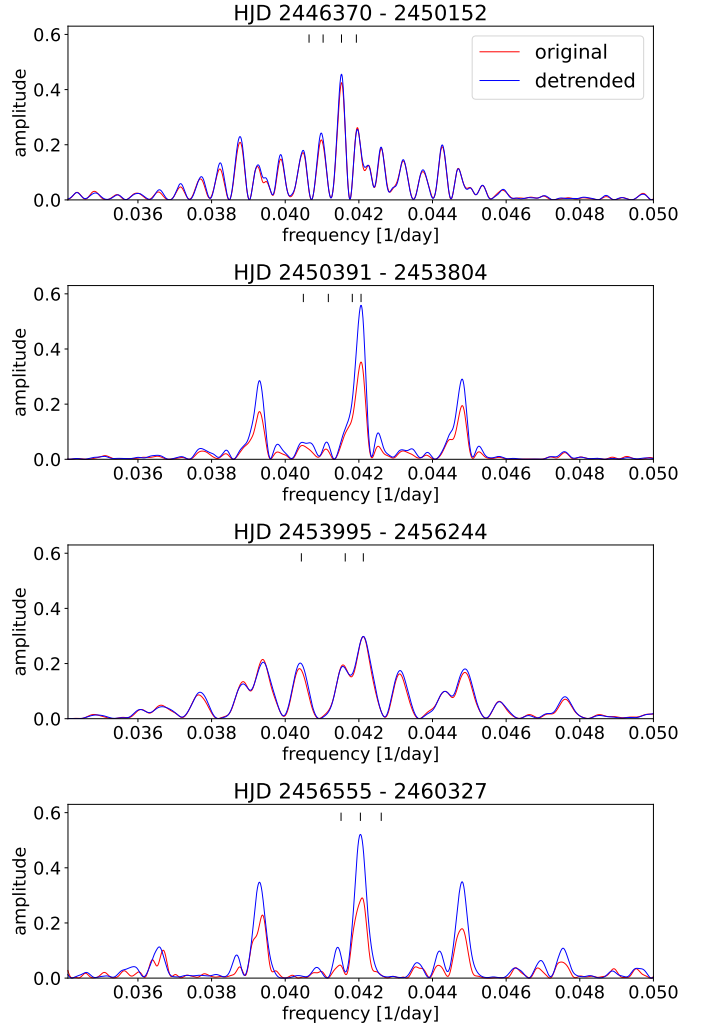


Fig. A.2. The rotation-related parts of the Lomb-scargle periodograms obtained for the four sub-seasons; see also Fig. 2. The ticks at the top of each panel are the locations of the periods listed in Table 2.